RESEARCH ARTICLE

Macromolecular Materials and Engineering
www.mame-journal.de

Melt Electrowriting of a Photo-Crosslinkable Poly(ϵ-caprolactone)-Based Material into Tubular Constructs with Predefined Architecture and Tunable Mechanical Properties

*Nele Pien, Michael Bartolf-Kopp, Laurens Parmentier, Jasper Delaey, Lobke De Vos, Diego Mantovani, Sandra Van Vlierberghe, Peter Dubruel, and Tomasz Jungst**

Melt electrowriting (MEW) is an additive manufacturing process that produces highly defined constructs with elements in the micrometer range. A specific configuration of MEW enables printing tubular constructs to create small-diameter tubular structures. The small pool of processable materials poses a bottleneck for wider application in biomedicine. To alleviate this obstacle, an acrylate-endcapped urethane-based polymer (AUP), using a poly(ϵ-caprolactone) (PCL) (molar mass: 20 000 g mol^{-1}) (AUP PCL20k) as backbone material, is synthesized and utilized for MEW. Spectroscopic analysis confirms the successful modification of the PCL backbone with photo-crosslinkable acrylate endgroups. Printing experiments of AUP PCL20k reveal limited printability but the photo-crosslinking ability is preserved post-printing. To improve printability and to tune the mechanical properties of printed constructs, the AUP-material is blended with commercially available PCL (AUP PCL20k:PCL in ratios 80:20, 60:40, 50:50). Print fidelity improves for 60:40 and 50:50 blends. Blending enables modification of the constructs' mechanical properties to approximate the range of blood vessels for transplantation surgeries. The crosslinking-ability of the material allows pure AUP to be manipulated post-printing and illustrates significant differences in mechanical properties of 80:20 blends after crosslinking. An in vitro cell compatibility assay using human umbilical vein endothelial cells also demonstrates the material's non-cytotoxicity.

1. Introduction

Additive manufacturing (AM) has proven itself to be a highly relevant tool for several application areas in the biomedical fields. AM is also an essential method in scientific research like bioprinting and biofabrication. In these disciplines, the hierarchical generation of tissue models and artificial grafting structures via automated processes is of utmost relevance for the progression of the field. The automation and computer assisted control of manufacturing that is introduced by AM techniques greatly benefited the progress being made in recent years. Key techniques include the process of ink jetting biomaterials, which enables for easy deposition of different materials and cell types, while also allowing to generate hollow constructs by dispensing cells into crosslinkable or hydrogel solutions.[1] Further techniques encompass the widely known and used extrusion printing which allows the direct deposition of cell laden materials, mostly hydrogels, into organized structures with larger dimensions and in a more time sensitive manner than ink

N. Pien, L. Parmentier, J. Delaey, L. De Vos, S. Van Vlierberghe, P. Dubruel
Polymer Chemistry & Biomaterials Research Group, Centre of Macromolecular Chemistry, (CMaC)
Ghent University
Krijgslaan 281 S4bis, Gent 9000, Belgium

The ORCID identification number(s) for the author(s) of this article can be found under https://doi.org/10.1002/mame.202200097

DOI: 10.1002/mame.202200097

N. Pien, D. Mantovani
Laboratory for Biomaterials and Bioengineering
CRC-I, Laval University
Pavillon Pouliot, Québec G1V 0A6, Canada

M. Bartolf-Kopp, T. Jungst
Department of Functional Materials in Medicine and Dentistry, Institute of Biofabrication and Functional Materials
University of Würzburg and KeyLab Polymers for Medicine of the Bavarian Polymer Institute (BPI)
Pleicherwall 2, Würzburg 97070, Germany
E-mail: tomasz.juengst@fmz.uni-wuerzburg.de

jetting.[2] The next step into higher organization and more precise construct geometries is the technique of vat polymerization-based bioprinting, including digital light processing (DLP), stereolithography (SLA), two-photon polymerization (2PP), and volumetric bioprinting, which capitalize on the precise curing of photosensible materials to polymerize in very delicate and also freestanding constructs.[3] All these techniques mostly use cells immersed in biocompatible materials, usually hydrogels, which are ideal for cell survival but often lack the mechanical rigidity that is found in native tissues. This point is relevant for the fabrication of hollow structures, especially blood vessel derivatives, as they are under constant and variable mechanical stress that they need to withstand for extended duration.

Melt electrowriting (MEW) is an emerging high-resolution, direct-writing additive manufacturing technique that is based on the deposition of an electro-hydrodynamically stabilized molten polymer jet onto a collector.[4] While conceptually comparable to the widely known principle of electrospinning, MEW offers the advantage of precisely depositing fibers in a well-defined pattern, allowing for intricate geometries to be realized.[5] In addition, a distinct advantage over conventional 3D printing (3DP) techniques, such as fused deposition modeling (FDM), is the smaller fiber diameter (i.e., 0.8–30 μm)[6] that can be achieved with MEW.[7]

At present, one of the challenges associated with the use of MEW is the limited availability of compatible materials.[8] The ideal material should not only be efficiently processable via MEW (i.e., low melting point, slow thermal/hydrolytic degradation, rapid solidification), but should also fulfill the requirements of the intended application. In the field of regenerative medicine, this implies that the final construct should elicit biocompatibility and cell-biomaterial interactions, have a controllable biodegradation rate and tunable mechanical properties that strongly depend on the requirements of each individual tissue.[9,10] Additionally, bioactive compounds bound to the surface or a controlled release from the biomaterial is favorable to generate an ideal growth environment for cells.[11,12] Generally, thermoplastic polymers are chosen for MEW as they are processable above a certain temperature, and solidify upon cooling.[13] Most polymers used for MEW have a high molar mass (MM), implying an increasing degree of chain entanglements, which is improving jet stability during the MEW process.[14] The current gold standard used in MEW is poly(ϵ-caprolactone) (PCL). This is mainly due to its semicrystalline and biodegradable properties, low melting temperature and rapid solidification, and the U.S. Food and Drug Administration (FDA) approval for multiple clinical applications.[15] However, it also has the drawback of being a hydrophobic polymer, featuring a high elongation at break but overall low elastic properties.[16] Due to this, PCL is attractive for biomedical applications including scaffolding and drug releasing material,[17] but is still lacking the ideal mechanical endurance to sustain tensile stress without plastic deformation to be the ideal material for applications in regenerative medicine.[18,19]

To overcome the limitations of conventional PCL, blending has been used to modify and also enhance the properties of the material.[19] Ideally, a blend should improve upon the favorable characteristics of a material while reducing the unwanted attributes of the educts. Several different materials from synthetic to organic have been used in the past to achieve more biocompatible or mechanically comparable blends with tissue models.[19] Problematic for the blending process are occurrences where the materials are not homogeneously mixing, leading to a phase separation or inhomogeneous distribution of the blended materials within the compound.[20]

A different approach to the challenge has been investigating the processability of other thermoplastic polymers, including commercially available polypropylene (PP) and poly(vinylidene fluoride) (PVDF),[21] as well as polymers specifically synthesized for MEW processing. Examples are the $(AB)_n$-type segmented copolymers, poly(2-oxazoline)s (POx), UV-crosslinkable polymers like poly(L-lactide-*co*-ϵ-caprolactone-*co*-acryloyl carbonate) (poly(LLA-ϵ-CL-AC)),[18] and PCL-based blends.[8,15] Despite those efforts, materials that enable printing constructs with tailorable mechanics and optimal mechanics for biomedical application are scarce. In addition, material blends that feature good results with MEW are prepared using solvents, hampering a transition into biomedical applications.

An interesting class of recently developed materials are acrylate-endcapped urethane-based polymers (AUP). One of their main benefits is that they can be designed by varying the different constituting building blocks.[22,23] Among other things, this enables the tunability of the mechanical properties of the developed material. Another key advantage of the AUP material is that it enables crosslinking in solid state.[24] In the past few years, AUP materials have been synthesized to serve various processing techniques and biomedical applications. For each specific application, the building blocks were selected in such a way that the material's properties would correspond to the application's requirements.[25–29] Initially, the AUP materials were based on a poly(ethylene glycol) (PEG) backbone in order to attain hydrogel-like properties.[22,23] These PEG-based AUPs have been processed successfully by 3D printing and electrospinning and have been used for meniscus tissue engineering (TE) and as wound dressings.[25–27] Next, AUPs with other backbones (e.g., PCL), exhibiting a variation in constituting building blocks (i.e., varying the spacer and end groups) were reported. To date, AUPs based on a PCL backbone with a MM of 2000 g mol^{-1} have been evaluated in 2-photon polymerization processing[24] and for tendon repair.[28,29]

Initially, MEW was established on planar collectors, but meanwhile, it has transitioned toward the fabrication of 3D tubular geometries[30,31] as various applications in regenerative medicine rely on such structures (including blood vessels, urethra, and ureters, intestine, nerve, etc.).[32] Therefore, research has been devoted toward the elaboration of methods to improve the design and fabrication of tubular scaffolds by exploiting specialized printer set-ups and mandrel collectors.[30,31] In this regard, the advantages of MEW (onto a rotating mandrel collector) offer great potential as they enable the generation of predefined architectures with high resolution, high porosity (i.e., >87%)[33] and interconnectivity due to the small fiber diameters. Especially, adaptable mechanical scaffold properties resulting in flexibility and scaffold compliance would further advance applicability of melt electrowritten structures for applications in regenerative medicine like vascular grafts but, to date, materials used in tubular MEW are even more limited as those used with planar collectors.[31]

To explore the potential of MEW as a processing technique to develop tubular scaffolds with a predefined architecture and tunable mechanical properties, we demonstrate a straightforward synthesis route for the development of an AUP material with a PCL backbone possessing a photo-crosslinkable moiety at each end and its processability with MEW. We show that postprocess crosslinking has a significant impact on the mechanical properties of the constructs produced by MEW compared to "commonly used" non-crosslinkable PCL. Blending of functionalized AUP PCL and nonmodified PCL enables tailoring mechanical properties as well as improving printing behavior. Both material as such, blends with unmodified medical grade PCL, and the MEW processed tubular constructs are evaluated with respect to their physicochemical properties. In addition, the cytocompatibility of the developed constructs is determined by an in vitro assay.

2. Experimental Section

2.1. Material Synthesis and Characterization

2.1.1. Material Synthesis

Endcap Synthesis: First, 1.2 equivalents of monoacrylated oligoethyleneoxide (OEOacr, Bisomer PEA6, GEO Specialty Chemicals) was added to 1 equivalent of isophorone diisocyanate (IPDI, Sigma-Aldrich) to react, at $T = 65$ °C for 2 h, after which the temperature was increased to 75 °C for 1 h 15 min. The synthesized endcap is further abbreviated as IPDI-OEOacr.

PCL Diol Synthesis: Secondly, the monomer (ϵ-caprolactone, 50 g, 483 mmol) (Sigma-Aldrich), catalyst (stannous octoate, 4 g, 10 mmol) (Sigma-Aldrich), solvent (dry toluene, 160 mL) (ChemLab Analytical), and initiator (ethylene glycol, 312 mg, 5 mmol) (Sigma-Aldrich) were added to a flame-dried Schlenk vial in an Argon-glovebox. The mixture was subjected to three freeze-thaw cycles. The Schlenk vial was placed in an oil bath at 100 °C while stirring and allowed to react for 24 h. The synthesized PCL diol was exploited as backbone for the acrylate-endcapped urethane-based polymer in a one-pot synthesis.

Before usage, toluene was dried by refluxing over sodium in the presence of benzophenone. ϵ-Caprolactone was purified by vacuum distillation over CaH_2, while ethylene glycol was purified by vacuum distillation and stannous octoate was used as received.

Acrylate-Endcapped Urethane-Based Material Synthesis: Next, acrylate-endcapped urethane-based PCL was synthesized by dissolving 2 equivalents of the IPDI-OEOacr in dry toluene in a 1:1 w:v ratio and adding the solution to the synthesized PCL diol (MM = 20 000 g mol^{-1}, synthesis vide supra) together with 300 ppm catalyst (stannous octoate). The resulting mixture was allowed to react overnight at $T = 75$ °C under an inert atmosphere. Then, the reaction mixture was precipitated in a 10-fold excess of cold hexane. The resulting precipitate was filtered and washed with cold hexane and dried in vacuo for 24 h. A schematic presentation can be found in Figure 2. For further annotations, the developed arylate-endcapped urethane-based material with a PCL backbone of 20k will be abbreviated by "AUP PCL20k" in the manuscript.

2.1.2. Material Characterization

Determination of the Acrylate Content and Molar Mass of the Developed AUP Using Nuclear Magnetic Resonance Spectroscopy: The developed AUP material was analyzed via nuclear magnetic resonance spectroscopy (^{1}H-NMR, Bruker Avance 400 MHz Spectrometer) at room temperature after dissolving the AUP in deuterated chloroform ($CDCl_3$, Euriso-Top) at a concentration of 10 mg mL^{-1}. For quantification of the acrylate concentration, dimethyl terephthalate (DMT, Sigma-Aldrich) was added to the NMR solutions of the AUPs, as an internal standard, at a concentration of 10 mg mL^{-1}. The calculations and corresponding equations can be found in the Supporting Information.

Evaluation of the Thermal Properties by Thermogravimetric Analysis (TGA) and Differential Scanning Calorimetry (DSC): Thermal stability was investigated by TGA (TA Instruments, Q50). First, the material pan was pyrolyzed with a Bunsen burner to remove remaining impurities. Next, the material (10 mg) was heated following a pre-programmed method of equilibration at 35 °C, ramping at a rate of 10 °C min^{-1} to 600 °C and cooling until equilibration at 350 °C. The software (TA Universal Analysis) registered the mass loss evolution as a function of the temperature.

The thermal properties of the AUP precursors were determined using conventional DSC (TA instruments, Q2000 DSC, Zellik, Belgium). 4–6 mg samples were placed into Tzero aluminum DSC pans and subsequently sealed using an aluminum Tzero lid. The samples were then placed into the device furnace and equilibrated at 45 °C prior to the start of the analysis. An initial heating cycle was applied to remove the thermal history of the samples by heating up the precursors up to 100 °C at a controlled rate of 10 °C min^{-1}. Next, the precursors were cooled down to 20 °C at a controlled cooling rate of 5 °C min^{-1} and equilibrated at 20 °C for 10 min. Next, the samples were heated again up to 100 °C at a controlled rate of 10 °C min^{-1}. The DSC thermograms recorded during the cooling and heating cycles were plotted as a function of the temperature.

Chemical Structure Analysis by FTIR Spectroscopy: FTIR spectroscopy analysis was conducted on an FTIR spectrometer (PerkinElmer Frontier FTIR mid-IR combined with a MKII Golden Gate set-up equipped with a diamond crystal from Specac) operating in Attenuated Total Reflection (ATR) mode. AUP spectra were recorded for the range of 700–4000 cm^{-1} with 8 scans.

Determination of Gel Fraction, Solvent Uptake Capacity, Crosslinking Efficiency, and Wettability: The crosslinked AUP samples were cut into disks (D: 8 mm, thickness: 1 mm) and weighed (*Wi*). The samples were incubated in deionized water for 24 h at room temperature and weighed in the swollen state (*Ws*). Next, the samples were removed, dried and weighed again (*Wf*). The solvent uptake capacities and gel fractions were determined using Equations (1) and (2), respectively

$$\text{Solvent uptake capacity } (SUC) = \frac{(W_s - W_f)}{W_f} \quad (1)$$

$$\text{Gel fraction } (GF) = \frac{W_f}{W_i} \quad (2)$$

The crosslinking efficiency (CE) was assessed by high resolution magic angle spinning (HR-MAS) ^{1}H-NMR spectroscopy on a Bruker Avance II 700 spectrometer. The spectrometer contains a HR-MAS probe which was equipped with a ^{1}H, ^{13}C, ^{119}Sn, and gradient channel. The spinning rate was set at 6 kHz. The freeze-dried samples were placed in a 4 mm zirconium oxide MAS rotor with Kel-F disposable inserts (50 µL). Next, 30 µL $CDCl_3$ was added to let the samples swell. Finally, the samples were homogenized prior to the measurement. A Kel-F cap was used to close the rotor. For the calculation of the Degree of Conversion (DC) from the NMR spectra[34] using Equation (3), the ethylene oxide peaks were chosen as reference peaks since they represent groups that do not participate in the crosslinking reaction, nor does this peak overlaps with the peaks of the blended virgin PCL

$$\text{Crosslinking efficiency } (CE)\,[\%] = \frac{\left(\frac{I_i}{I_{ri}} - \frac{I_e}{I_{re}}\right)}{\left(\frac{I_i}{I_{ri}}\right)} \times 100\% \quad (3)$$

Static contact angles were measured in air at room temperature with an OCA20 optical contact angle measuring system (DataPhysics, Germany). The contact angle measurements were determined by the sessile drop test, and a Laplace Young Fitting Circle method. A droplet of 0.5 µL Milli-Q ultrapure water was suspended on the surface using a microsyringe with a dosing rate of 1 µL s^{-1}. Water contact angle measurements were performed in triplicate ($n = 3$).

Evaluation of the Mechanical Properties of Crosslinked AUP Samples: The UV-crosslinked AUP samples (100 wt% initial precursor concentrations) were cut into dogbone-shaped samples (1 mm thickness, 30 mm gage length, 4 mm width). Next, the tensile properties of the crosslinked AUP dogbone-shaped samples were determined at room temperature using a universal testing machine (Tinius Olsen) equipped with a 500 N load cell. A preload force of 0.3 N was applied and the specimens were tested at a cross-head velocity of 10 mm min^{-1}. Young's moduli were calculated from the initial slope of the stress–strain plots on 4 replicates.

Rheological Measurements on Crosslinked AUP Discs: The UV-crosslinked AUP samples (100 wt% initial precursor concentration) were cut into disks ($D = 14$ mm, thickness = 1 mm). Storage (G') and loss moduli (G'') of the AUP samples were determined via an Anton Paar Physica MCR 301 rheometer using a parallel-plate set-up (top plate diameter: 15 mm) as a function of the frequency (1–100 Hz). During the tests, the normal force was kept at 0.8 N in order to ensure contact between the measuring system and the sample. The tests were performed at a strain (<0.5%) which was in the linear viscoelastic region of the samples, predetermined by the strain-controlled oscillatory tests (data not shown). The rheological measurements were done in triplicate.

2.2. Material Processing using Melt Electrowriting

2.2.1. Material Selection for MEW Processing

For the blended materials, an automated microcompounder system (MC 5, Xplore Instruments BV) was utilized. To the blends, 0.1 wt% TPO-L as photoinitiator was added with respect to the amount of AUP PCL20k material in the blend or pure batch of material. The following ratios have been realized by compounding at 85 °C for 30 min at 50 rpm: 1) AUP PCL20k, 2) AUP PCL20k:PCL 80:20, 3) AUP PCL20k:PCL 60:40, 4) AUP PCL20k:PCL 50:50, and 5) PCL (Purac Purasorb PC 12–1.18 dl g^{-1} density –80 g mol^{-1}).

2.2.2. Device and Processing Parameters

Tubular constructs of AUP or PCL, as well as blends of the two materials were processed with a custom-made melt electrowriting device with a cylindrical and interchangeable collector. The motorization is based on an Aerotech axis system (PRO115) and uses the A3200 (Aerotech) software suite as coding and machine operating interface. A modified code has been developed similar to previous work[35] to move the collector in translational as well as rotational directions to allow precise fiber placement onto a steel mandrel in predetermined winding angles. For the extrusion of materials, polypropylene cartridges, and 22G flat tipped needles (Nordson EFD) were used in all experiments. Printing parameters were optimized for each individual blend of material and maintained throughout the experimental process. A close-up image of the printing nozzle during MEW is shown in Figure S1 (Supporting Information), both for the extrusion of AUP PCL20k and for the extrusion of PCL.

2.3. Tubular Construct Characterization

2.3.1. Photo-Crosslinking of Developed Tubular Constructs

A postprocessing UV treatment was performed on the developed AUP/PCL tubular constructs by ultraviolet (UV-A) irradiation at 2×5 mW cm^{-2} (Philips TL 0W/08 P8 T5/BLB lamps in the holder of Bi-Sonic Technology Corp.; model 8B-230 HB; 250–450 nm range) for 30 min.[28]

2.3.2. Visualization of the Tubes' Micro- and Macroarchitecture

The tubular constructs were analyzed using a SEM device (Crossbeam CB 340 SEM, Carl Zeiss) for evaluation of the fiber diameter and the general fiber morphology. Videos to illustrate the mechanical behavior of the different AUP/PCL blend tubular constructs have been recorded on a mirrorless interchangeable-lens camera (Nikon Z 4, Nikon Corporation) with a macrolens (AF Micro-Nikkor 200 mm 1:4D IF-ED, Nikon Corporation).

2.3.3. Physicochemical Characterization of the Tubular Constructs

Determination of Gel Fraction, Solvent Uptake Capacity, and Crosslinking Efficiency of the Developed Tubular Constructs: The GF, SUC, and CE of crosslinked tubular constructs were determined using the equations in Section 2.1.2.

Influence of Melt Electrowriting on the Molar Mass of the Material: The number average molar mass (M_n), the weight average molar mass (M_w), and the polydispersity ($Đ$) were determined by conventional gel permeation chromatography (GPC)

using polystyrene standards (Agilent Technologies, weight average molar mass range: 580–1 930 000 g mol^{-1}). The polymers were dissolved (10 mg mL^{-1}) in chloroform (Biosolve, analytical grade) and filtered through a membrane with a 0.45 mm pore size. The analyses were performed by liquid chromatography (Alliance Waters 1515 isocratic pump with Waters 717plus Autosampler and Waters 2414 Refractive Index Detector) equipped with PLGel Mixed-D polystyrene divinylbenzene GPC columns (353 PSI). The sample components were separated by the GPC columns based on their molecular size in solution and detected by a refractive index detector.

Evaluation of Mechanical Properties of the Developed Tubular Constructs by Uniaxial Tensile Testing: To determine the mechanical properties of the fabricated tubular constructs, a customized fixation setup on a dynamic mechanical testing device (ElectroForce 5500, TA Instruments) was used. The sample mounting construction allowed two metal pins to be introduced into the luminal cavity of the constructs and applied radial tensile force during the testing procedure (Figure S2, Supporting Information). Samples were measured in a 100 cycle waveform setup with a peak displacement of 18% strain in reference to the inner tube diameter. Evaluation of the construct measurements has been done after initial hysteresis subsided and the peak force stabilized over several cycles. Pull to failure quantification used the identical setup and displaced the construct over a distance of 10 mm, equivalent to 330% strain. Both non-UV treated, and UV-treated tubular MEW constructs have been evaluated in triplicate.

2.3.4. Biological Evaluation of Developed Tubular Constructs Using Human Umbilical Vein Endothelial Cells

The biocompatibility of the various materials (AUP PCL20k, PCL, and their combinations 50:50, 60:40, and 80:20) was evaluated through indirect contact in vitro biological assays. Human umbilical vein endothelial cells (HUVECs) (Lonza) were cultured under standard incubator culture conditions (37 °C, 5% CO_2) with supplemented endothelial cell growth medium-2 (EGM-2) (Promocell) additionally supplemented with 1% Pen/Strep (Sigma). Medium was changed every 2–3 days. The cells were split until a confluency of 80–90% and used at passage 5.

The MEW tubes were sterilized through incubation in 70 v/v% EtOH for 24 h with a change after 12 h. Subsequently, the samples were exposed to UV-C irradiation for 2 h followed by incubation at 37 °C in culture medium at a concentration of 1.125 mL mg^{-1} of material during 1, 3, and 7 days. Short-term component leaching was then evaluated on seeded cells both in terms of cell viability as well as cell proliferation.

To this end, 10 000 HUVECs were seeded into a well of a 96-well plate. The cells were allowed to attach for 24 h awaiting the addition of the medium in contact with the manufactured tubes for 1, 3, or 7 days. This test was performed in triplicate. Cells seeded on tissue culture plastic with the addition of standard supplemented EGM-2 medium was included as reference.

HUVEC cell proliferation was assessed through an MTS (3-(4,5-dimethylthiazol-2-yl)-5-(3-carboxymethoxyphenyl)-2-(4-sulfophenyl)-2H-tetrazolium) (Abcam) assay which was applied in a 20 v/v% ratio with culture medium to the cells. Reduction of the component into its formazan dye by the HUVECs during 2 h of incubation at 37 °C in the dark enables the quantification of metabolic activity through absorbance measurements at 490 nm (BioTek Instruments, EL800 Universal Microplate Reader with GEN5 software).

A live-dead viability assay was performed through the addition of 0.2 v/v% calcein-acetylmetoxyester (Ca-AM) (Sigma) and 0.2 v/v% propidium iodide (PI) (Sigma) in phosphate buffered saline (PBS). The cells were visualized after 10 min of incubation in the dark with a fluorescence microscope (Olympus IX81 with software Xcellence Pro) with a green fluorescent protein (GFP) filter for living cells and a texas red (TxRed) filter for dead cells.

2.4. Statistical Analysis

All data were analyzed using GraphPad Prism 8.0.2. A one-way or two-way ANOVA test were performed followed by a Tukey post-test. The symbols representing the different significant levels are indicated on the graphs (i.e., ns = $p > 0.05$; * = $p \leq 0.05$; ** = $p \leq 0.01$; *** = $p \leq 0.001$).

3. Results and Discussion

To successfully engineer a specific tissue model, research is focusing on material design and advances in processing. A combination of the emerging technology of MEW and the design of novel materials provides a promising approach for the fabrication of mechanically adjustable tubular constructs for applications in regenerative medicine. In the present work, we hypothesize that our photo-crosslinkable PCL-based polymer is a suitable material feedstock to be applied in MEW. The presence of photo-crosslinkable moieties in the AUP and the possibility to easily blend with conventional PCL enables fine-tuning of material properties. A physico-chemical characterization was performed, before evaluating the material's potential for the use in in MEW of tubular constructs. In addition, the tubular samples were analyzed with respect to physico-chemical and biological properties after fabrication. A schematic overview of the research conducted in this study is visualized in **Figure 1**.

3.1. Synthesis and Physico-Chemical Analysis

There are some key requirements to consider when designing a material for MEW. One important aspect includes the melting and glass transition temperature which enable processing of the material in a molten state. Ideally, the material is easily processable above its melt temperature due to reduced melt viscosity, lacks pronounced thermal degradation and is rapidly solidifying after processing.[13] These properties can be achieved by a sufficiently high molar mass[36] so that enough chain entanglements are present which result in viscoelastic melt properties that improve processing via MEW and help generating a stable jet.[14]

3.1.1. Material Synthesis

As described in the introduction, AUPs are a class of materials that can be designed by varying the constituting building

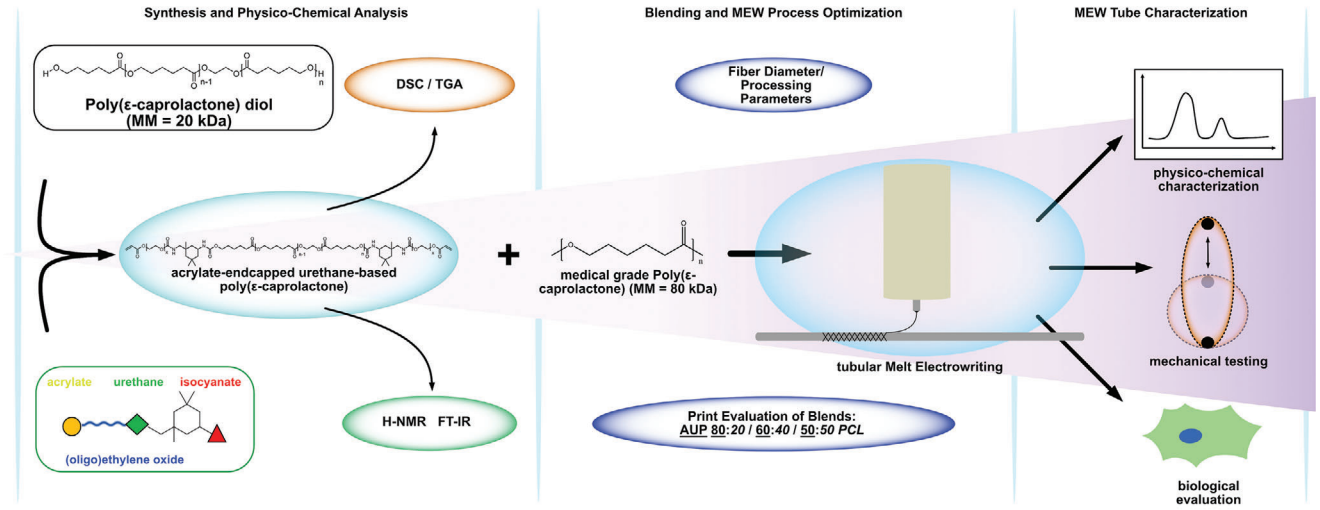

Figure 1. Experimental overview of the synthesis and process evaluation.

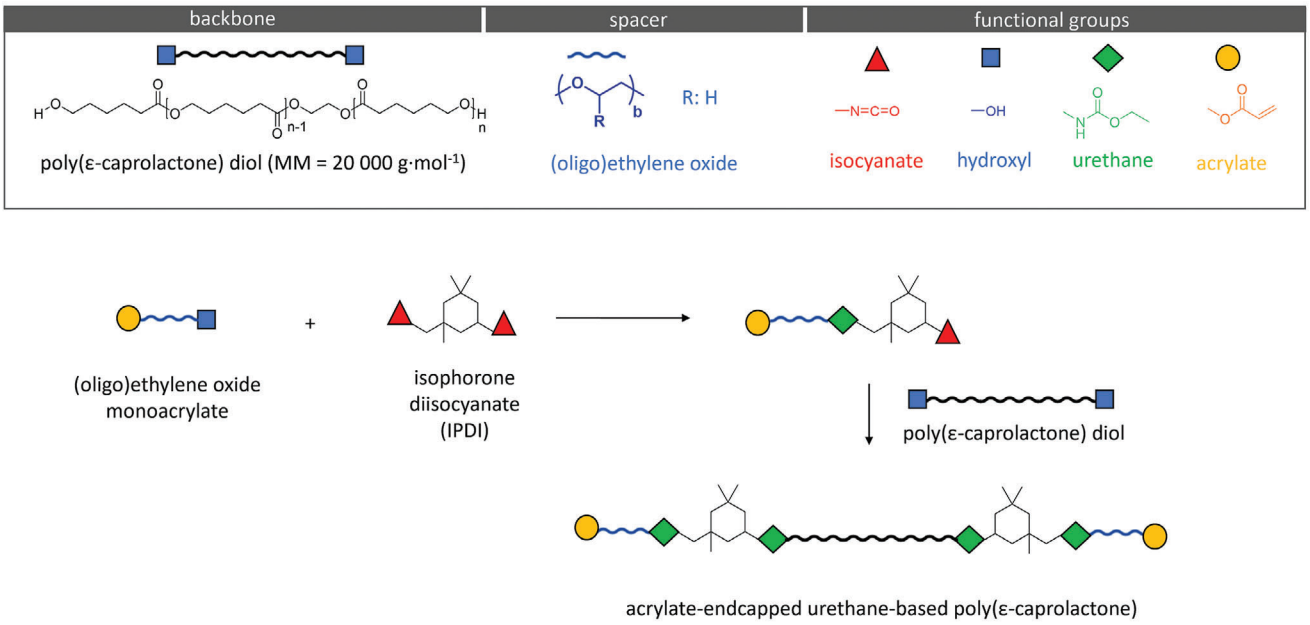

Figure 2. Synthesis of an acrylate-endcapped urethane-based polymer (AUP) constituting a poly(ε-caprolactone) backbone, an (oligo)ethylene oxide spacer and a monoacrylate endgroup.

blocks (**Figure 2**). With respect to the material requirements of MEW, an AUP with a PCL backbone of a higher molar mass (MM = 20 000 g mol^{-1}) compared to previously reported PCL-based AUPs (MM = 530 and 2000 g mol^{-1})[24,28] was synthesized. In addition to the higher MM aiming at improving the material's MEW processing potential, the acrylate endgroups enable crosslinking of the developed constructs after processing.

3.1.2. Material Characterization

The chemical structure of the newly developed AUP polymer was analyzed via FT-IR (Figure S3, Supporting Information) and proton nuclear magnetic resonance (^{1}H-NMR) spectroscopy. Via the latter technique, the acrylate concentration (0.036 mmol g^{-1}), the molar mass of the backbone (26 168 g mol^{-1}) and the molar mass of the AUP material (27 076 g mol^{-1}) were determined. The FT-IR spectrum revealed the characteristic absorption bands corresponding to N–H stretching (3330 cm^{-1}) and the amide II (1530 cm^{-1}) band confirming that the urethanization reaction successfully proceeded throughout the synthesis. The spectrum also confirmed the complete conversion of the isocyanate groups (i.e., disappearance of the peak corresponding to N=C=O at 2260 cm^{-1}) that react with the hydroxyl moieties of the PCL diol and those of the end-capping agents (Figure S4). The absorption

Table 1. MEW printing parameters for the different materials processed. V_{eff} = effective velocity, d_m = distance to mandrel, ZHS (Z-Axis Height Shift) = strand layer height. Fiber diameter as measured on SEM images. Melt viscosity and shear rate of the materials and material blends as obtained by compounding at 50 rpm, $T = 85$ °C, and $t = 30$ min. ± indicates the standard deviation.

Material	Temperature [°C]	Pressure [bar]	Voltage [kV]	V_{eff} [mm min^{-1}]	d_m [mm]	ZHS [µm]	Fiber diameter [µm]	Melt viscosity [kPa s]	Shear rate [kN m^{-2}]
AUP PCL20k	70	0.55	5.5	511	4.5	15	66.70 ± 34.22	0.26	4.1
80:20	80	0.60	4.4	707	3.5	17	36.21 ± 6.74	0.28	4.2
60:40	89	0.60	4.4	707	3.5	17	18.81 ± 1.76	0.32	5.1
50:50	89	0.60	4.4	707	3.5	14.5	17.02 ± 1.43	0.34	5.6
PCL	89	0.65	5.8	500	3.55	14.5	13.46 ± 0.23	0.35	5.7

bands at 1635 and 810 cm^{-1} correspond to the C=C stretch and the =CH_2 out-of-plane deformation of the acrylate groups.[24] The connection of the flexible, mono-acrylate spacer to the backbone using a di-isocyanate linker enables great mobility of the reactive groups, and exhibit excellent solid-state photo-reactivity.[24,37]

The thermal stability and properties of AUP PCL20k was evaluated with TGA and DSC analyses, respectively. The degradation onset point was located at 256.27 °C, as anticipated, well above the processing temperature used for MEW. In addition, 1% mass loss was recorded at a temperature of 193.28 °C, whereas this was 227.22 and 276.93 °C for 5% and 50% mass loss, respectively. This is in accordance to previously reported thermal stability of PCL-based AUPs (with lower MM and/or other endgroups).[28] From DSC analysis, a melting temperature of 53.64 °C ($\Delta H = 67.86$ J g^{-1}), a crystallization temperature of 30.42 °C ($\Delta H = 71.25$ J g^{-1}) and a glass transition temperature of −47.54 °C were obtained. Both the Tm and the Tg of the developed AUP PCL20k material are slightly lower compared to those of pure PCL (i.e., Tm = 60 °C and the Tg = −60 °C).[38,39] This can be explained by the plasticizing influence of the oligo(ethyene oxide) spacer in the AUP material. As such, the PCL-based AUP with a MM of 20 000 g mol^{-1} is processable using MEW[33,40] due to higher viscosity and melt temperature than AUPs generated with lower MM (data not shown), that allow for a quicker solidification. As shown in Section 3.2 **Table 1**, the recorded viscosity of AUP PCL 20 000 g mol^{-1} (0.26 kPa s) was found to be lower than PCL (0.35 kPa s).

The physico-chemical properties of the crosslinked AUP PCL20k was assessed by means of a gel fraction (GF) and solvent uptake capacity (SUC) assay as well as HR-MAS NMR spectroscopy to determine the crosslinking efficiency (CE). A gel fraction of 99.5 ± 0.6% and a crosslinking efficiency of 79.9% were obtained. This indicated that the AUP PCL20k was effectively crosslinked. As anticipated for PCL-based materials, evaluation of the swelling properties indicated a limited solvent uptake capacity (0.93 ± 0.25).[24,28] The wettability of the AUP PCL20k, PCL and their blends (80:20, 60:40, 50:50) has been evaluated using static contact angle measurements. The results (Figure S5, Supporting Information) indicated a significant lower ($p < 0.05$) contact angle between AUP PCL20k and PCL, with a contact angle of 77.7 ± 3.3° and 88.4 ± 0.8°, respectively. Also, the 80:20 blend showed a statistically significant lower contact angle compared to PCL ($p < 0.05$). This implies that the AUP PCL20k and the 80:20 blend have a higher wettability compared to PCL.

The mechanical properties of the crosslinked precursors were evaluated via rheology and via tensile testing. Figure S6 (Supporting Information) shows the tensile testing set-up and an example of a stress-strain curve obtained from uniaxial testing on a photo-crosslinked dogbone-shaped AUP sample. The rheological measurements on crosslinked AUP discs revealed a storage modulus G' of 387.81 ± 27.47 kPa and a loss modulus G'' of 48.71 ± 7.08 kPa. Upon tensile testing, the urethane-based polymer showed an ultimate force of 70.97 ± 10.73 N, a maximum stress of 13.23 ± 1.17 MPa with a corresponding strain of 5.67 ± 1.16%. The stress-strain relationship indicated a Young's modulus of 321.44 ± 21.23 MPa. This evidenced improved mechanical strength compared to the PCL-based AUPs with a lower MM of 2000 g mol^{-1} that showed a Young's modulus of 6.30 ± 0.30 MPa.[24] Moreover, the developed AUP PCL 20 000 g mol^{-1} indicated a higher ultimate force and maximum stress and a lower corresponding strain when compared to the lower MM AUP variant. Based on these results, it can be concluded that in case of PCL-based AUPs, an increase in MM mainly leads to stronger but less flexible materials. However, it was anticipated that the lower amount of acrylate endgroups present in the AUP PCL 20 000 g mol^{-1} (i.e., 0.04 mmol g^{-1}) compared to AUP PCL 2000 g mol^{-1} (i.e., 0.55 mmol g^{-1}) would lead to less strongly crosslinked materials upon increasing the MM. It is hypothesized that the effect of the higher MM leading to more chain entanglements and thus increased mechanical strength, is overcoming the less strongly crosslinking abilities due to lower amount of acrylates. In addition, the increase in MM of the PCL diol backbone can also influence the crystallinity of the AUP. This hypothesis is based on similar observations as reported by Grosvenor et al.[41] They observed an increased Young's modulus and tensile strength when increasing the MM of PCL, up till a certain point whereafter it starts deceasing again, and concluded this was due to crystallinity and chain entanglements.[41] When comparing the developed AUP PCL20k to commercially available PCL, a similar maximum stress (13.58 ± 0.83 MPa), a higher maximum strain (10.62 ± 1.18%), and a 10-fold lower Young's modulus (18.90 ± 5.15 MPa) was observed for the nonmodified PCL. These findings illustrate the tunability of mechanical properties when both materials are blended in different ratios.

3.2. Blending and MEW Process Optimization

After characterization of the developed PCL-based AUP (MM = 20 000 g mol^{-1}), the potential for its application as MEW processable material was considered. The key processing parameters for MEW include i) mass flow rate, ii) collector speed, iii) electric field, and iv) melt temperature. Viscosity and

conductivity of the fluid define the properties of the molten polymer and need to be considered when choosing process conditions.[42] It should also be stated that upon changing one of these key process parameters, the other parameters will also be influenced, and thus a proper optimization of all parameters in different combinations is required. The process parameters were adjusted until a suitable setting could be elaborated to achieve constant material flow and construct layering.

After achieving a stable material processing parameter set, the construct specifications were tested and optimized. Following predefined specifications were chosen for tubular construct generation: the length of the construct was set to 11.56 mm, the number of fiber layers on top of each other was set to 20, the angle which the fibers are aligned in relation to the longitudinal axis (winding angle) was 70°, and the number of turning points (pivot points) of the construct was 8. Further description of the printing variables can be found in the work of McColl et al.[35]

A printability evaluation of the pure AUP material revealed vastly different characteristics compared to commercially available, non-modified PCL. The developed AUP PCL20k was more prone to electrical discharge phenomena, known as arcing, at a higher incidence than regular PCL. This was compensated by reducing the applied voltage and by increasing the printhead distance to the collector. Overall, it was difficult to retain fiber morphology directly after printing, resulting in fiber merging and fusion, requiring lower melt temperatures to allow quicker solidification of the material. This slow solidification characteristic also manifested in very inhomogeneous fibers as well as attraction between the previously placed fibers and newly deposited, causing deviations from the programmed printing path. Nevertheless, it was possible to create constructs that resembled the programmed geometry (**Figure 3**).

To improve the printing properties of AUP PCL20k, blending with non-modified PCL was performed. This enables combining the favorable printing behavior of medical grade PCL with benefits of the developed photo-crosslinkable AUP material. It is assumed that the higher molar mass of PCL improves printability and fiber deposition while AUP enables modification of the material´s mechanical properties via photo-crosslinking. In MEW, combining different materials is usually performed by mixing those in a dissolved state. Such an approach has already been undertaken in studies like the one by Hochleitner et al.[43,44] where blending of polymers to create a co-polymer for MEW was applied in order to alter the material properties. Toluene was utilized as a solvent to generate the blend. In contrast, blending was performed using a compounder to physically mix the PCL and AUP to create a blend of materials in this study. To evaluate how much PCL was needed to improve printing properties of AUP PCL20k and the resulting mechanics, several ratios with different composition of AUP PCL20k:PCL were chosen (80:20 and 60:40). Furthermore, a blend of 50:50 was added as previous studies with AUP have shown beneficial electrospinning behavior using this material ratio.[28] Materials were blended for 30 min at 85 °C and afterwards transferred into printing cartridges. Melt viscosity and shear rate were recorded during blending, allowing for an initial evaluation of the blends and planning of process parameters. Lower viscosities usually require adaptation towards less material flow (reduced voltage/pressure) or faster collector speeds to properly distribute the material to achieve straight and homogeneous fibers.[14] Table 1 illustrates the printing parameters chosen to process the blends. Overall, printability of the blends increased with higher ratios of PCL within the blend. A sweet spot could be reached at 60:40 where the fiber morphology and fiber diameter variation were already very comparable to commercial PCL. The blend with a 50:50 ratio showed a similar result. A slight increase in fiber diameter of 4–5 µm was the most pronounced difference between the 60:40/50:50 blend and pure PCL. The 80:20 ratio still showed increased fiber merging and required adjustments of printing parameters. Overall processability of AUP PCL20k with MEW is possible, and with the blending of AUP PCL20k and commercial PCL, a beneficial printing behavior could be demonstrated.

An overview with representative images of each blend-ratio-group is depicted in Figure 3. The images were taken as a basis for the evaluation of the fiber diameter of the different blends, an integral value to assess the quality of MEW-processed materials.[45] A clear trend is visible regarding scaffold morphology: the scaffolds become more amorphous and inconsistent in their fiber distribution and overall structure when more AUP PCL20k is present in the material, with the most prominent effect observed in the pure AUP PCL20k sample. This effect can also be correlated with the increase in fiber diameter and the homogeneity of the produced fibers (PCL 13.46 ± 0.23 µm, AUP PCL20k 66.7 ± 34.22 µm). The scaffolds made with pure AUP PCL20k and the ones with an AUP PCL20k:PLC ratio of 80:20 led to fiber morphologies which started to lose their clear appearance as single fibers stacked on top of each other. This is clearly visible at the crossover points of deposited fibers (Figure 3, 3rd column). With higher amounts of AUP PCL20k (ratios of 80:20 and higher), fibers begin to merge with each other as soon as they are stacked, indicating a slow solidification of the material after extrusion. Adjustments to the printing temperature were necessary to fabricate the structures (Table 1). The cause of this effect can potentially stem from a thermodynamically different behavior of AUP PCL20k compared to PCL. It is hypothesized that a combination of factors including the differences in melt viscosity and shear rate (Table 1), which were found to be lower for AUP PCL20k (0.26 kPa s) compared to PCL (0.35 kPa s), and the slightly lower melting temperature of AUP PCL2k (T_m = 53.64 °C) compared to PCL (T_m = 60 °C) can foster the effect of fiber fusing.

To quantitatively illustrate the difference between the mechanical properties of the printed constructs made with varying AUP PCL20k:PCL ratios, a manual compression test has been conducted (Video S1, Supporting Information). Clearly visible is the increasing stiffness and resistance to compression for increased AUP PCL20k content compared to pure PCL, indicating the effective alteration of the material properties after processing, and successful post-processing crosslinking of the materials. The pure AUP PCL20k sample is not able to withstand the compression and breaks immediately while the blends all remain undamaged.

3.3. MEW Tube Characterization

3.3.1. Physico-Chemical Characterization

Determination of Gel Fraction, Solvent Uptake Capacity, and Crosslinking Efficiency of the Developed Tubular Constructs: The

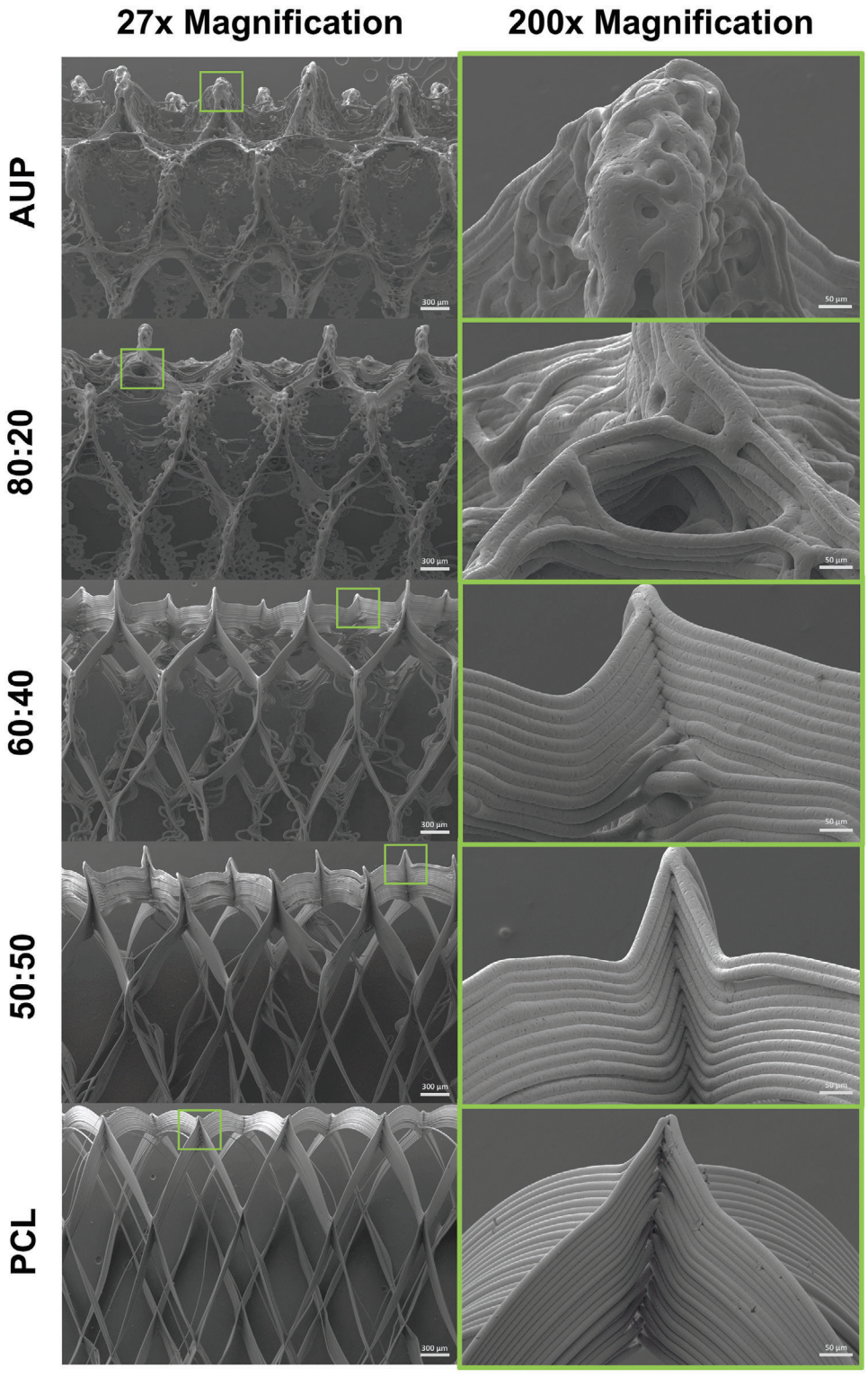

Figure 3. SEM images of the MEW processed tubes of PCL and AUP, as well as the selected blends of AUP:PCL at 27× and 200× magnification. The green boxes indicate the location of the 200× magnification on the SEM image with 27× magnification.

Table 2. Gel fraction (GF), solvent uptake capacity (SUC), and crosslinking efficiency (CE) of AUP PCL20k, AUP PCL20k:PCL blends, and PCL.

Material	GF		SUC		CE
	[%]	SD	[–]	SD	[%]
AUP PCL20k	98.4	2.5	1.3	0.4	79.9
80:20	97.4	0.9	0.9	0.1	69.0
60:40	95.4	1.6	0.2	0.1	49.6
50:50	99.0	5.9	0.1	0.1	35.4
PCL	100.0	0.0	0.3	0.1	—

Table 3. Determination of the M_n, M_w, and polydispersity ($Đ$) of AUP, PCL, and their blends, before and after MEW processing, using gas permeation chromatography. M_n = number average molar mass, M_w = weight average molar mass, and $Đ$ = polydispersity index determined via GPC analysis.

Material	M_n [g mol^{-1}]		M_w [g mol^{-1}]		$Đ$ [—]	
	Before	After	Before	After	Before	After
AUP PCL20k	23 072	22 127	31 504	30 684	1.37	1.39
80:20	23 652	25 107	45 920	45 231	1.94	1.80
60:40	30 226	32 129	61 354	64 347	2.03	2.00
50:50	26 369	34 531	78 038	72 411	2.96	2.10
PCL	76 946	65 520	130 381	108 820	1.69	1.66

gel fractions of the tubes made by MEW from AUP PCL20k, PCL, and their blends all exceed 95% (**Table 2**). For pure AUP PCL20k, a GF of 98.4 ± 2.5% was obtained, giving a first indication that processing with MEW did not influence the material's ability to crosslink effectively. This implies that almost no leaching out of potential noncrosslinked material constituting the developed tubes will occur when applied in tissue engineering. In addition, the material's ability to crosslink was confirmed by calculating the percentage of consumed acrylate groups (i.e., crosslinking efficiency, CE) obtained from HR-MAS NMR spectroscopy indicating a crosslinking efficiency (CE) of 79.9% (Table 2). Moreover, the data showed that the CE clearly decreased with a decrease of AUP PCL20k in the blend. For the 50:50 and 60:40 blends, a CE lower than 50% was obtained, implying an incomplete conversion of the available reactive groups. The 50:50 blend only possessed a CE of 35.4%, which is due to the limited number of crosslinkable moieties.

For applications that rely on the mechanical properties of the constructs, it is important that the solvent uptake capacity (SUC) of the developed tubes is as low as possible to avoid excessive swelling of the construct to ensure that the scaffolds do not lose their shape and structure during cell culture. In accordance with the SUC of pure, non-printed AUP PCL20k (i.e., 0.93 ± 0.25 before processing), similar values were obtained for the processed AUP PCL20k tubes (i.e., 1.30 ± 0.42) (ns. $p > 0.05$). Very small SUC (<1.30 ± 0.42) was obtained for the developed MEW tubes, independently of the blend ratio. As anticipated, for pure PCL constructs, shape and structure were perfectly maintained after contact with water as demonstrated by high GF and low SUC during a timeframe of 24 h.

Influence of Melt Electrowriting on the Molar Mass of the Material: As anticipated, the GPC measurements confirmed that the MEW processing technique did not influence the molar masses of the AUP and PCL (**Table 3**). For AUP PCL20k, the number average molar mass (M_n) was around 23 072 g mol^{-1} and the weight average molar mass (M_w) was around 31 504 g mol^{-1} (with a $Đ$ < 1.5) which corresponds to the MM that was determined using ^{1}H-NMR spectroscopy (i.e., 27 076 g mol^{-1}). The GPC measurements indicated a MM of the commercially available PCL was similar to that reported in the technical sheet of the supplier (MM of 120 000 g mol^{-1}). Depending on the AUP:PCL ratio in the blend, both the M_n and M_w increased with an increasing PCL content in the blend. This was as expected because of the higher MM of PCL compared to AUP PCL20k. The differences in MM of the different blends have an influence on the printing parameters and optimization (as discussed in Section 3.2) as well as on the mechanical properties of the developed tubes (vide infra). It was also observed that the polydispersity increased when more PCL was blended in, moreover, $Đ$ was higher in all blends compared to $Đ$ of both the pure AUP PCL20k and pure PCL. This confirmed that the observed distribution of the blends is less uniform ($Đ$ = 1) upon blending in more PCL. The $Đ$ of pure AUP PCL20k, PCL, and the blend with a ratio of 80:20 could still be defined as moderate, whereas a $Đ$ of more than 2 as is the case for 60:40 and 50:50 could be defined as a broad polydisperse distribution.

3.3.2. Mechanical Properties of MEW Tubes

To investigate the mechanical properties of the fabricated tubular constructs, unidirectional mechanical tests were performed. The constructs were analyzed by a dynamic radial tensile experiment over a cycle count of 100 at a strain of 18% to simulate conditions close to those that blood vessel experience during physiological conditions.[46–49] Further, a series of pull to failure tests has been conducted to evaluate the behavior of the constructs under elevated influence of tensile force.

The graphs depicted in Figure S7 (Supporting Information) show the plots for representative samples of the different material blends of AUP PCL20k and PCL as well as the pure samples as force per displacement before and after UV-induced postprocess crosslinking of the acrylates within AUP PCL20k containing samples. **Figure 4** depicts stress/strain plots of the different samples. Young's moduli, peak force and retained force were calculated according to a method described in literature for the analysis of radially tested tubular constructs and are shown in Figure 4C–F.[50] All samples, except the pure, non-crosslinked AUP samples which broke apart during the first cycle, could be tested. Interestingly, the crosslinked AUP samples did not break during the first cycle but only started to break over the course of the testing protocol. Even though the force reduced at each cycle, a minimal force was maintained at the end of 100 cycles (Figure S8, Supporting Information).

Evaluating the maximum tensile stress exhibited by the constructs (Figure 4F) revealed the rather brittle nature of the AUP PCL20k material. Successive increase in the amount of blended PCL into the compounded materials elevated the levels of ultimate tensile stress close to the values recorded for pure PCL. The

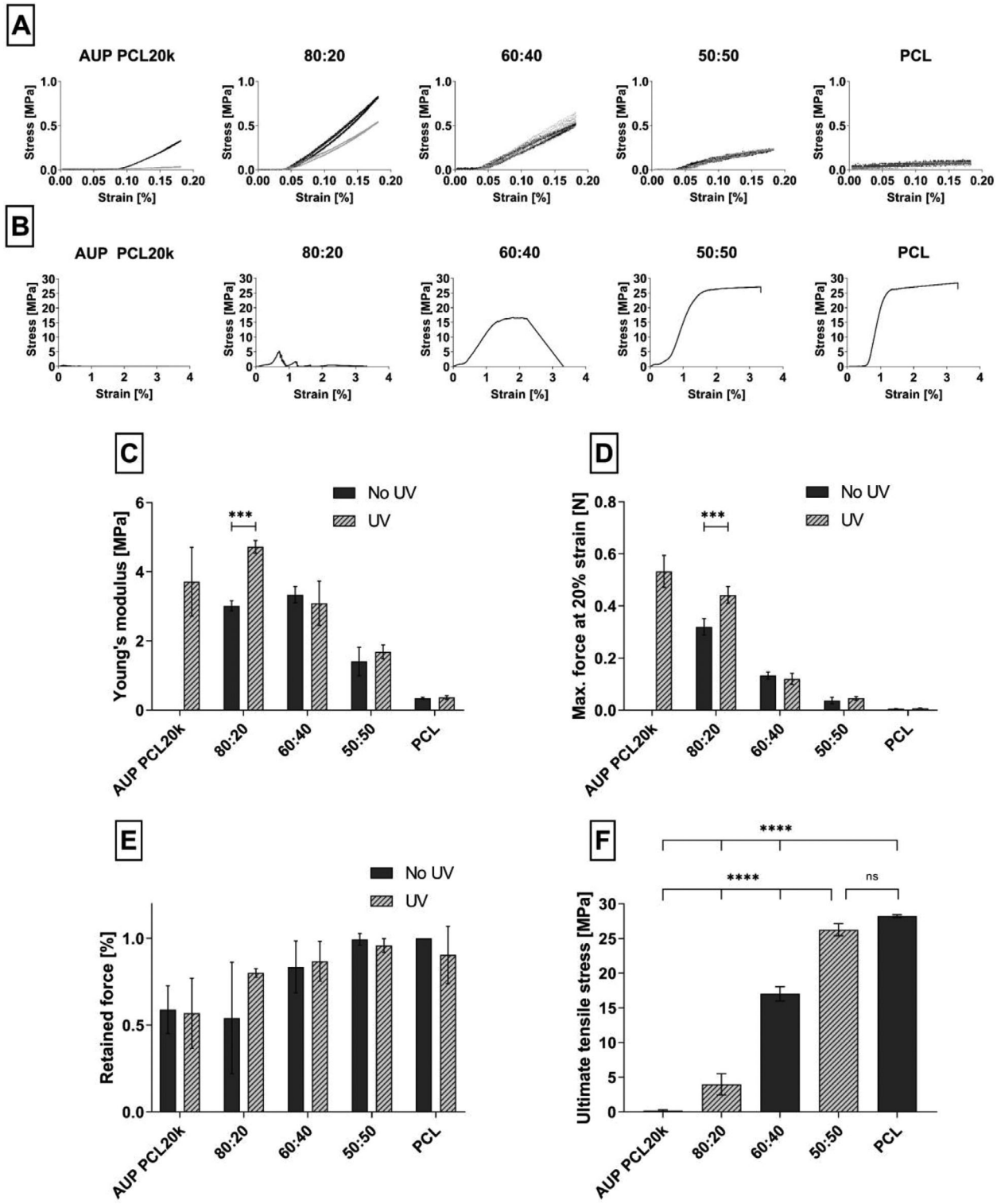

Figure 4. Mechanical evaluation of tubular constructs: (A) + (B): Stress [MPa] versus strain [%] plots obtained from a single construct via uniaxial tensile testing data on MEW processed tubes (AUP, AUP:PCL ratios of 80:20, 60:40, and 50:50, and PCL): A) Representative graphs of cyclic radial tensile testing of single constructs after initial hysteresis resided. Compared are constructs with (black) and without (gray) postprocessing UV irradiation. B) Representative graphs of singular construct pull to failure testing. Constructs were pulled to 330% strain to elucidate their failure point. C–F) depict mean and SD values of mechanical data analysis: (C) Young's moduli [MPa]. (D) Max. force at 20% strain [N]. (E) The mean retained force [%], calculated by the difference of force at the beginning and at the end of measurement. (*** = $p < 0.0001$). (F) Ultimate stress [MPa] of the developed MEW tubes (after UV crosslinking) in AUP PCL20k, PCL, and their blends (80:20, 60:40, 50:50) as obtained from uniaxial tensile testing until failure. (****: $p < 0.0001$, ns: $p > 0.05$).

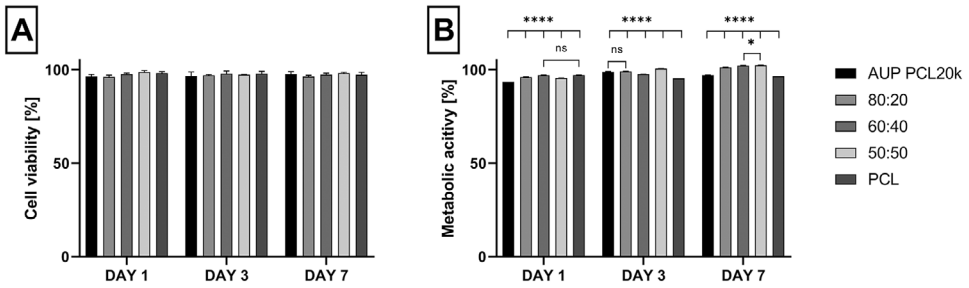

Figure 5. In vitro biocompatibility assay using human umbilical vein endothelial cells on day 1, 3, and 7: A) cell viability (no significant differences, $p > 0.05$). B) Metabolic activity (**** = $p < 0.0001$ between all groups per day except if indicated with another symbol: ns = $p > 0.05$ or * = $p < 0.05$).

50:50 blend showed no significant difference compared to pure PCL regarding stress at break. On the one hand, AUP PCL20k showed a very small overall value in the amount of force required for a break of the construct. This might arise due to the overall fragile constructs and the testing protocol, which was set up to displace at slightly higher velocities than compared to the cyclic evaluation, leading to a more pronounced failure of the constructs early on. On the other hand, this reinforces the benefit of blending the material with PCL to attenuate this material characteristic. Figure 4B depicts representative curves recorded during the pull to failure test. It is noticeable that the higher amount of PCL leads to the characteristic plastic deformation of PCL at elevated stresses before reaching a plateau of stagnant force increase where the material is undergoing a ductile failure behavior. Higher amounts of AUP PCL20k lead to a more brittle failure behavior of the material.

A clear trend is visible with respect to the declining amount of peak force depending on the amount of AUP PCL20k present in the blends. The highest recorded value was observed for the UV-crosslinked pure AUP PCL20k group (Figure 4D). The only significant difference when comparing UV-treated versus non-UV treated values (within one blend) could be recorded for the 80:20 blend samples ($p < 0.0001$). The high content of AUP PCL20k within this blend enables a more effectively crosslinked network, due to increased acrylate group interaction, that leads to an increased mechanical strength. This is in agreement with the HR-MAS data (see Section 3.3.2a), where a crosslinking efficiency of more than 50% was found for the 80:20 blend, and below 50% for the 60:40 and 50:50 blends.

The Young's moduli exhibit comparable trends as described for the peak force. The only significant difference between non-crosslinked and crosslinked samples is present in the 80:20 blend group (Figure 4C) ($p < 0.0001$). When comparing Young's moduli with values from literature, the blended samples all range in the relevant window of 2–4 MPa which corresponds to average values from human saphenous vein (1.77 ± 1.2 MPa), radial artery (3.68 ± 2.05 MPa) and coronary artery, which are in the range from 1.5[51,52] to 4 MPa,[53] depending on the specimen and test protocol used. With that, the blending allowed the manufactured constructs to be closer to human blood vessels regarding their young's modulus, whereas constructs made only from PCL do not reach these ranges. As anticipated, the differences in mechanical properties of the pure AUP PCL20k and PCL (as discussed in Section 3.1.2) also lead to differences in mechanical properties of the developed tubular constructs based on the different materials. By blending and varying the blend ratio, this resulted in achieving a range of Young's moduli in between the higher Young's modulus of the AUP PCL20k and the lower Young's modulus of the PCL, and thus tuneability in mechanical properties.

The graphs for all groups show very narrow hysteresis loops (Figure S7, Supporting Information), indicating very little plastic deformation over the course of the cyclic measurement. A closer look at the peak force for all samples during 100 cycles (Figure 4E) reveals a decline of peak force values during cycling testing. The decline can be attributed to the internal material properties, adjusting to the external tensile force until an equilibrium between fiber extension and orientation according to the applied force is reached.[54,55] Due to the crosslinked network, the amount of AUP PCL20k in the blend corresponds with a higher force decay over the course of the 100 cycles, while a higher PCL ratio shows little to no decay.[56]

Regarding differences between non-UV and UV-treated samples, only the 80:20 group shows a 32% difference in peak force between the start and end of the measurement (Figure 4D). This can be caused by the very brittle nature of the AUP PCL20k material that leads to breaking within the sample at the beginning of the measurement, resulting in an overall lower force, while the formed crosslinked bonds allow the material to withstand the applied tensile force better. The 50:50 blends perform best regarding force retention as well as having a noticeable increase in Young's modulus compared to pure PCL. Relevant observations for potential application in vascular regeneration or replacement are the small hysteresis loops shown during the testing, especially as the investigated displacement area is larger than physiological values for cyclic extension during systole of comparable small diameter blood vessels.[49] Additionally, there is only a very small decay of force over the whole 100 cycles of tensile testing. These results indicate the potential for long term mechanical dilatation and that the constructs are suited to withstand physiological stresses.

3.3.3. Biological Evaluation

The in vitro biocompatibility of the developed MEW tubes was evaluated via an MTS assay and Ca-AM/PI staining. To this end, HUVECs were assessed on days 1, 3, and 7 after indirect contact with the materials, which is a common evaluation for testing of biocompatibility.[57,58] The rationale behind the choice of HU-

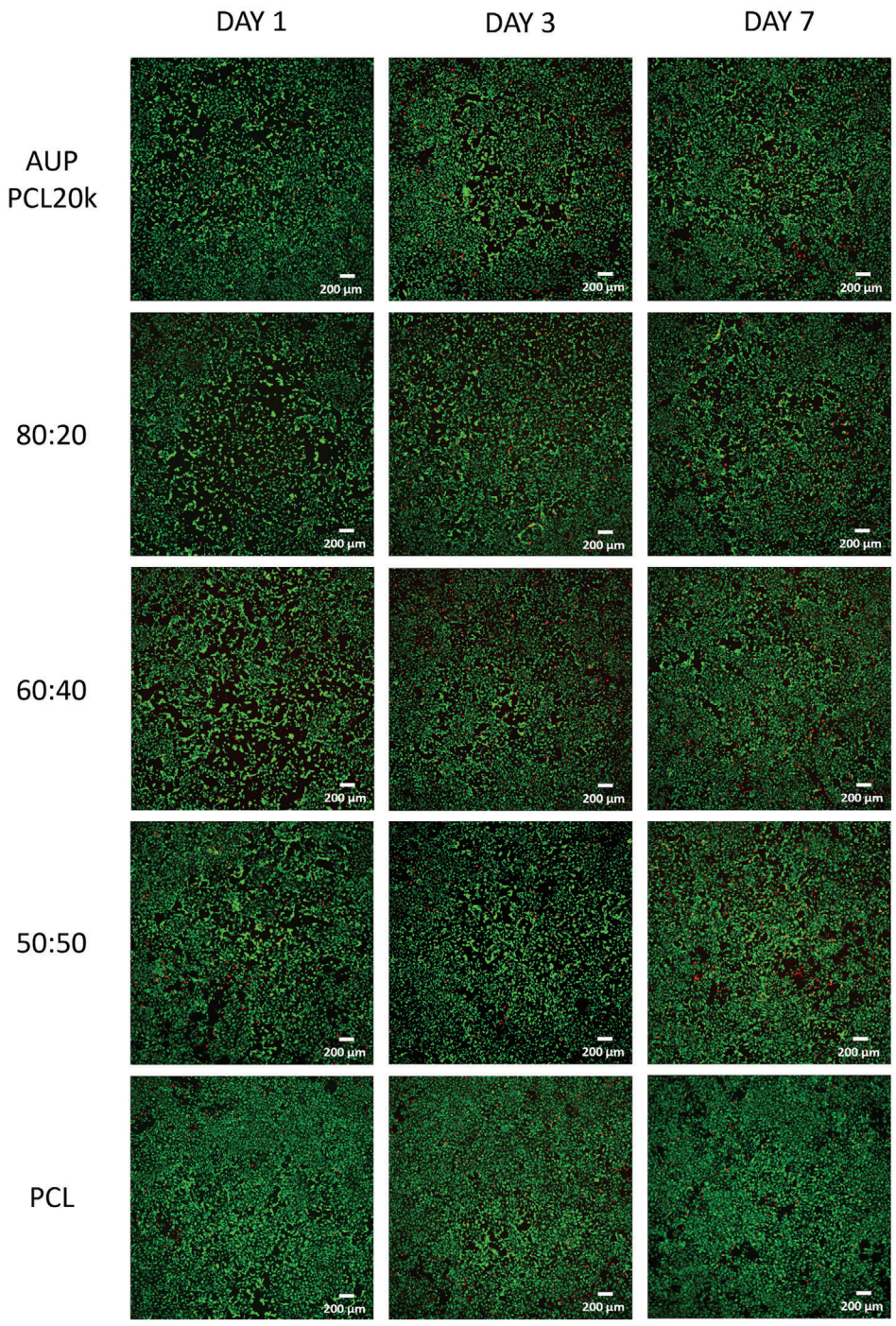

Figure 6. Live/dead (Ca-AM/PI) staining images of HUVECs in an indirect contact assay for AUP, PCL, and their blends at day 1, day 3, and day 7.

VECs as cell type is because one of the potential applications of the developed MEW tubes is their function as a reinforcement in in vitro vascular models. In blood vessels, endothelial cells, in the experimental evaluation represented by HUVECs, together with fibroblasts and smooth muscle cells form the majority of cell types present in vasculature[59] and therefore a logic option to test herein for their viability after exposure to the constructs.

Following the ISO 10993-5:2009(E), a biomaterial and its leaching components are noncytotoxic, if the viability is above 70%.[60] As indicated in **Figure 5**A, the HUVEC viability at day 1, 3, and 7 remained well above 70% for AUP PCL20k, PCL, and their blends (i.e., >95%). The live/dead staining images can be found in **Figure 6**. In addition, an excellent metabolic activity was observed (Figure 5B). Thus, it can be concluded that the

developed MEW tubular constructs do not show any cytotoxicity toward the HUVECs and could be further evaluated for their use as reinforcements constructs in vascular tissue engineering applications.

4. Conclusions

In conclusion, this work presents the application of an acrylate-endcapped urethane-based polymer (AUP), synthesized with a straightforward synthesis route to introduce photo-crosslinkable moieties to a PCL backbone, for MEW of tubular constructs with adaptable mechanical properties. Processing with MEW did not result in degradation of the material and the photo-crosslinking capacity was preserved. Blending with commercially available PCL helped improving fiber morphology and homogeneity. At the same time, altering the mechanical properties of the created construct by adjusting the blend ratios was possible. This enables tailor-made construct characteristics for different applications and their corresponding specific mechanical requirements. In vitro assay using HUVECs revealed noncytotoxic behavior of the AUP material demonstrating its relevance in biomedical applications.

Supporting Information

Supporting Information is available from the Wiley Online Library or from the author.

Acknowledgements

The authors would like to acknowledge Prof. José Martins of the NMR department for helping with the NMR measurements. The work of N.P. was supported by a Vanier Canada Graduate Scholarship. N.P. would like to acknowledge the financial support of the Research Foundation Flanders (FWO) under the form of a travel grant for her research stay at the FMZ lab (K201221N)). D.M. would like to acknowledge the continuous support by the Natural Science and Engineering Research Council of Canada, and the contribution of the *Fonds de Recherche du Québec sur les Natures et Technologies*, and the Canada Foundation for Innovation. P.D. and S.V.V. would like to acknowledge the financial support of the Research Foundation Flanders (FWO) under the form of research grants. M.B.-K. would like to thank the Deutsche Forschungsgemeinschaft (DFG, German Research Foundation -Project No. 326998133-TRR 225 – subproject Z01) for financial support. The DFG also supported the project with a "'State Major Instrumentation Programme"' funding for the SEM Zeiss Crossbeam 340 (INST 105022/58-1 FUGG) that enabled analysis of the samples. In addition, the authors thank the European Union for support on printing strategies (European Fund for Regional Development – EFRE Bayern, Bio3D-Druck project 20-3400-2-10). T.J. acknowledges the European Union for funding via the European Union's Horizon 2020 research and innovation program under Grant Agreement No. 874827.

Open access funding enabled and organized by Projekt DEAL.

Conflict of Interest

The authors declare no conflict of interest.

Author Contributions

N.P. and M.B.-K. contributed equally to this work. N.P.: Conceptualization; Data curation; Formal analysis; Funding acquisition; Investigation; Methodology; Project administration; Resources; Software; Validation; Visualization; Roles/Writing – original draft; Writing – review & editing. M.B.-K.: Conceptualization; Data curation; Formal analysis; Funding acquisition; Investigation; Methodology; Project administration; Resources; Software; Validation; Visualization; Roles/Writing – original draft; Writing – review & editing. L.P.: Data curation; Formal analysis; Methodology; Visualization; Roles/Writing – original draft. Jasper Delaey: Data curation; Formal analysis; Methodology; Roles/Writing – original draft. Lobke De Vos: Data curation. D.M.: Funding acquisition; Supervision; Writing – review & editing. P.D.: Funding acquisition; Supervision; Writing – review & editing. S.V.V.: Conceptualization; Funding acquisition; Investigation; Methodology; Project administration; Resources; Validation; Visualization; Writing – review & editing. T.J.: Conceptualization; Funding acquisition; Investigation; Methodology; Project administration; Resources; Validation; Visualization; Writing – review & editing.

Data Availability Statement

The data that support the findings of this study are available from the corresponding author upon reasonable request.

Keywords

acrylate-endcapped urethane-based polymer (AUP), melt electrowriting (MEW), photo-crosslinking, physicochemical characterization, tubular constructs

Received: February 11, 2022
Revised: April 14, 2022
Published online: May 22, 2022

[1] X. Li, B. Liu, B. Pei, J. Chen, D. Zhou, J. Peng, X. Zhang, W. Jia, T. Xu, *Chem. Rev.* **2020**, *120*, 10793.
[2] T. Jiang, J. G. Munguia-Lopez, S. Flores-Torres, J. Kort-Mascort, J. M. Kinsella, *Appl. Phys. Rev.* **2019**, *6*, 011310.
[3] W. L. Ng, J. M. Lee, M. Zhou, Y.-W. Chen, K.-.X. A. Lee, W. Y. Yeong, Y.-F. Shen, *Biofabrication* **2020**, *12*, 022001.
[4] T. D. Brown, P. D. Dalton, D. W. Hutmacher, *Adv. Mater.* **2011**, *23*, 5651.
[5] A. Hrynevich, B. Ş. Elçi, J. N. Haigh, R. Mcmaster, A. Youssef, C. Blum, T. Blunk, G. Hochleitner, J. Groll, P. D. Dalton, *Small* **2018**, *14*, 1800232.
[6] G. Hochleitner, T. Jüngst, T. D. Brown, K. Hahn, C. Moseke, F. Jakob, P. D. Dalton, J. Groll, *Biofabrication* **2015**, *7*, 035002.
[7] J. Kim, E. Bakirci, K. L. O'neill, A. Hrynevich, P. D. Dalton, *Macromol. Mater. Eng.* **2021**, *306*, 2000685.
[8] G. Hochleitner, E. Fürsattel, R. Giesa, J. Groll, H.-W. Schmidt, P. D. Dalton, *Macromol. Rapid Commun.* **2018**, *39*, 1800055.
[9] L. S. Nair, C. T. Laurencin, *Prog. Polym. Sci.* **2007**, *32*, 762.
[10] M. Martina, D. W. Hutmacher, *Polym. Int.* **2007**, *56*, 145.
[11] D. Belotti, C. Foglieni, A. Resovi, R. Giavazzi, G. Taraboletti, *Int. J. Biochem. Cell Biol.* **2011**, *43*, 1674.
[12] K. Klimek, G. Ginalska, *Polymers* **2020**, *12*, 844.
[13] A. Nadernezhad, M. Ryma, H. Genç, I. Cicha, T. Jüngst, J. Groll, *Adv. Mater. Technol.* **2021**, *6*, 2100221.
[14] F. M. Wunner, P. Mieszczanek, O. Bas, S. Eggert, J. Maartens, P. D. Dalton, E. M. De-Juan-Pardo, D. W. Hutmacher, *Biofabrication* **2019**, *11*, 025004.
[15] J. C. Kade, P. D. Dalton, *Adv. Healthcare Mater.* **2021**, *10*, 2001232.
[16] S. S. Sabet, A. A. Katbab, *J. Appl. Polym. Sci.* **2009**, *111*, 1954.
[17] M. A. Woodruff, D. W. Hutmacher, *Prog. Polym. Sci.* **2010**, *35*, 1217.

[18] F. Chen, G. Hochleitner, T. Woodfield, J. Groll, P. D. Dalton, B. G. Amsden, *Biomacromolecules* **2016**, *17*, 208.
[19] M. Abedalwafa, F. Wang, L. Wang, C. Li, *Rev. Adv. Mater. Sci.* **2013**, *34*, 123.
[20] S. Wachirahuttapong, C. Thongpin, N. Sombatsompop, *Energy Procedia* **2016**, *89*, 198.
[21] S. Florczak, T. Lorson, T. Zheng, M. Mrlik, D. W. Hutmacher, M. J. Higgins, R. Luxenhofer, P. D. Dalton, *Polym. Int.* **2019**, *68*, 735.
[22] A. Arslan, H. Van Den Bergen, P. Roose, D. Bontinck, S. Van Vlierberghe, P. Dubruel, *Patent WO2020/094621 A1*, **2020**.
[23] P. Dubruel, S. Van Vlierberghe, A. Houben, H. Van den Bergen, P. Roose, D. Bontinck, *Patent WO 2017/005613*, **2017**. https://www.google.com/patents/WO2017005613A1?cl=en
[24] A. Arslan, W. Steiger, P. Roose, H. Van Den Bergen, P. Gruber, E. Zerobin, F. Gantner, O. Guillaume, A. Ovsianikov, S. Van Vlierberghe, P. Dubruel, *Mater. Today* **2021**, *44*, 25.
[25] A. Houben, N. Pien, X.i Lu, F. Bisi, J. Van Hoorick, M. N. Boone, P. Roose, H. Van Den Bergen, D. Bontinck, T. Bowden, P. Dubruel, S. Van Vlierberghe, *Macromol. Biosci.* **2016**, *16*, 1883.
[26] M. Minsart, A. Mignon, A. Arslan, I. U. Allan, S. Van Vlierberghe, P. Dubruel, *Macromol. Mater. Eng.* **2021**, *306*, 2000529.
[27] A. Mignon, D. Pezzoli, E. Prouvé, L. Lévesque, A. Arslan, N. Pien, D. Schaubroeck, J. Van Hoorick, D. Mantovani, S. Van Vlierberghe, P. Dubruel, *React. Funct. Polym.* **2019**, *136*, 95.
[28] N. Pien, I. Peeters, L. Deconinck, L. Van Damme, L. De Wilde, A. Martens, S. Van Vlierberghe, P. Dubruel, A. Mignon, *Mater. Sci. Eng. C* **2021**, *119*, 111504.
[29] I. Peeters, N. Pien, A. Mignon, L. Van Damme, P. Dubruel, S. Van Vlierberghe, D. Mantovani, V. Vermeulen, D. Creytens, A. Van Tongel, S. Schauvliege, K. Hermans, L. De Wilde, A. Martens, *J. Orthop. Res.* **2021**, *40*, 750.
[30] T. D. Brown, A. Slotosch, L. Thibaudeau, A. Taubenberger, D. Loessner, C. Vaquette, P. D. Dalton, D. W. Hutmacher, *Biointerphases* **2012**, *7*, 13.
[31] T. Jungst, M. L. Muerza-Cascante, T. D. Brown, M. Standfest, D. W. Hutmacher, J. Groll, P. D. Dalton, *Polym. Int.* **2015**, *64*, 1086.
[32] N. Pien, S. Palladino, F. Copes, G. Candiani, P. Dubruel, S. Van Vlierberghe, D. Mantovani, *Cells Tissues Organs* **2021**, 128.
[33] A. Youssef, A. Hrynevich, L. Fladeland, A. Balles, J. Groll, P. D. Dalton, S. Zabler, *Tissue Eng., Part C* **2019**, 367.
[34] S. Van Vlierberghe, B. Fritzinger, J. C. Martins, P. Dubruel, *Appl. Spectrosc.* **2010**, *64*, 1176.
[35] E. Mccoll, J. Groll, T. Jungst, P. D. Dalton, *Mater. Des.* **2018**, *155*, 46.
[36] A. Daneshfar, S. L. Edwards, L. F. Dumée, L. Kong, T. C. Hughes, *ACS Appl. Polym. Mater.* **2021**, *3*, 1890.
[37] A. Houben, P. Roose, H. Van Den Bergen, H. Declercq, J. Van Hoorick, P. Gruber, A. Ovsianikov, D. Bontinck, S. Van Vlierberghe, P. Dubruel, *Mater. Today Chem.* **2017**, *4*, 84.
[38] V. R. Sinha, K. Bansal, R. Kaushik, R. Kumria, A. Trehan, *Int. J. Pharm.* **2004**, *278*, 1.
[39] H. Wang, M. Domingos, F. Scenini, *Rapid Prototyp. J.* **2018**, *24*, 731.
[40] R. Sanchez Diaz, J.-R. Park, L. L. Rodrigues, P. D. Dalton, E. M. De-Juan-Pardo, T. R. Dargaville, *Adv. Mater. Technol.* **2021**, *7*, 2100508.
[41] M. Grosvenor, *Int. J. Pharm.* **1996**, *135*, 103.
[42] T. M. Robinson, D. W. Hutmacher, P. D. Dalton, *Adv. Funct. Mater.* **2019**, *29*, 1904664.
[43] G. Hochleitner, F. Chen, C. Blum, P. D. Dalton, B. Amsden, J. Groll, *Acta Biomater.* **2018**, *72*, 110.
[44] G. Hochleitner, M. Kessler, M. Schmitz, A. R. Boccaccini, J. Teßmar, J. Groll, *Mater. Lett.* **2017**, *205*, 257.
[45] G. Hochleitner, A. Youssef, A. Hrynevich, J. N. Haigh, T. Jungst, J. Groll, P. D. Dalton, *Biofabrication* **2016**, *17*, 159.
[46] P. Zilla, D. Bezuidenhout, P. Human, *Biomaterials* **2007**, *28*, 5009.
[47] N. R. Tai, H. J. Salacinski, A. Edwards, G. Hamilton, A. M. Seifalian, *Br. J. Surg.* **2000**, *87*, 1516.
[48] D. B. Camasão, D. Mantovani, *Mater. Today Bio.* **2021**, *10*, 100106.
[49] G. Konig, T. N. Mcallister, N. Dusserre, S. A. Garrido, C. Iyican, A. Marini, A. Fiorillo, H. Avila, W. Wystrychowski, K. Zagalski, M. Maruszewski, A. L. Jones, L. Cierpka, L. M. De La Fuente, N. L'heureux, *Biomaterials* **2009**, *30*, 1542.
[50] X. Li, H. Zhao, *J. Biomater. Appl.* **2019**, *33*, 1017.
[51] H. Chen, G. S. Kassab, *J. Biomech.* **2016**, *49*, 2548.
[52] A. Karimi, M. Navidbakhsh, A. Shojaei, S. Faghihi, *Mater. Sci. Eng. C* **2013**, *33*, 2550.
[53] F. Fazal, S. Raghav, A. Callanan, V. Koutsos, N. Radacsi, *Biofabrication* **2021**, *13*, 032003.
[54] X. Gu, *Opto-Mech. Fiber Opt. Sensors Res. Technol. Appl. Mech. Sens.* **2018**, 49. https://doi.org/10.1016/B978-0-12-803131-5.00003-9.
[55] Y. C. Fung, S. C. Cowin, *J. Appl. Mech.* **1994**, *61*, 1007.
[56] J. P. Trotignon, J. Verdu, C. Martin, E. Morel, *J. Mater. Sci.* **1993**, *28*, 2207.
[57] J. J. Green, J. Shi, E. Chiu, E. S. Leshchiner, R. Langer, D. G. Anderson, *Bioconjug. Chem.* **2006**, *17*, 1162.
[58] Y. Cao, Y. Gong, L. Liu, Y. Zhou, X. Fang, C. Zhang, Y. Li, J. Li, *J. Appl. Toxicol.* **2017**, *37*, 1359.
[59] *Blood Vessels and Lymphatics in Organ Systems*, (Eds: L. OPIE, D. I. Abramson, P. B. Dobrin), Academic Press, Orlando, FL **1984**; *J. Mol. Cell. Cardiol.* **1986**, *18*, 335. https://doi.org/10.1016/S0022-2828(86)80418-7.
[60] ISO 10993-5:2009(en) Biological evaluation of medical devices – Part 5: Tests for in vitro cytotoxicity, **2009**.

